Hybrid Stainless Steel Girder for Bridge Construction

Tetsuya Yabuki, Yasunori Arizumi, Tetsuhiro Shimozato, Samy Guezouli, Hiroaki Matsusita, Masayuki Tai

Abstract—The main object of this paper is to present the research results of the development of a hybrid stainless steel girder system for bridge construction undertaken at University of Ryukyu. In order to prevent the corrosion damage and reduce the fabrication costs, a hybrid stainless steel girder in bridge construction is developed, the stainless steel girder of which is stiffened and braced by structural carbon steel materials. It is verified analytically and experimentally that the ultimate strength of the hybrid stainless steel girder is equal to or greater than that of conventional carbon steel girder. The benefit of the life-cycle cost of the hybrid stainless steel girder is also shown.

Keywords—Smart structure, hybrid stainless steel members, ultimate strength, steel bridge, corrosion prevention.

I. INTRODUCTION

SUSTAINING long life of structures is becoming of much concerning in structural engineering [1]. The local governments administrate 68% of the steel bridges used in Japan as shown in Fig. 1. The majority of local bridges have the girder span with less than 15m. Remarkable increase in the maintenance costs of those short span bridges places an enormous financial burden on local governments. Therefore, it is desired to reduce the maintenance costs of local bridges by realizing a minimum maintenance bridge with short spanning. When compared to conventional steels, stainless steel has much higher corrosion resistance, lower maintenance costs, greater durability, and more aesthetically appealing [1]. Considering these capabilities, it will be spectacular to use stainless steels in bridges [2], [3]. Namely, bridge girders constructed from welded thin-walled stainless steel plates are eco-friendlier, aesthetically and will result lower life-cycle costs when compared to conventional steel girders.

Hitherto, stainless steels have rarely been used in bridge constructions because of the material costs. However, in constructing a bridge, it is essential to account not only the initial costs comprised of manufacturing, transport and erection costs, but also the maintenance costs expended to achieve the long life of the important infrastructure. Especially, the primary costs for the maintenance to sustain the life of steel girder bridge in local areas are expenses expended to prevent the

T. Yabuki is with the Integrated Innovation Center, University of Ryukyu, Nishihara, 903-0129, Japan (phone: 81-98-895-8701, e-mail: yabuki@tec.u-ryukyu.ac.jp).

Y. Arizumi is with the Faculty of Engineering, University of Ryukyu, (phone: 81-98-895-8664, e-mail: arizumi@tec.u-ryukyu.ac.jp).

T. Shimozato is with the Faculty of Engineering, University of Ryukyu, (phone: 81-98-895-8666, e-mail: simozato@tec.u-ryukyu.ac.jp).

S. Guezouli is with Départment de Génie Civil et Urbain, Institut National Sciences Appliquées, Rennes, France (e-mail: samy.guezouli@insa-rennes.fr)

H. Matsusita is with Hitachi Zosen Corporation, Sakae 592-8331, Japan (e-mail: matsushita@hitachizosen.co.jp)

M. Tai is with the Faculty of Engineering, University of Ryukyu, (phone: 81-98-895-8659, e-mail: tai@tec.u-ryukyu.ac.jp).

generation of corrosion. Considering the essential demand in local areas, the authors are developing a smart bridge girder system to be suitable for short-spanning, i.e. a hybrid stainless steel girder for bridge construction as shown in Fig. 2. The superstructure of the bridge is one-box-shaped girder. The outside of the girder exposed to the external air is composed of stainless steel materials and the inside of the girder is constituted by structural carbon steel elements such as stiffeners, ribs, stringers, cross-beams, diagonal bracings, gusset plates, etc. Hence, the girder is composed of hybrid members of stainless steel and carbon steel. The corrosion proofing and the cost reduction are achieved by this hybrid treatment.
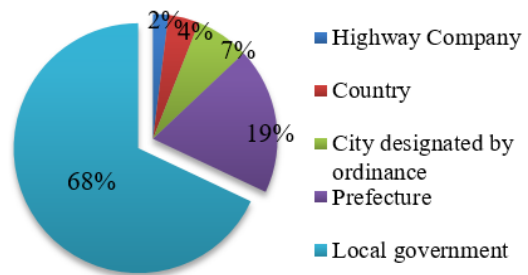

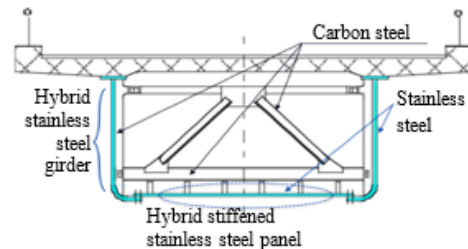Fig. 1 Administrators of steel bridges used in Japan

Fig. 2 Basic geometry of hybrid stainless steel bridge girder

First, this paper clarifies the background for corrosion proof of the hybrid stainless steel girder. Then, the practicability of the hybrid stainless steel girder in bridge construction is evaluated by comparing to ordinary carbon steel girders with respect to the ultimate strengths and the life-cycle costs.

II. CONCEPT FOR CORROSION PROOFING

A. Corrosion Behaviour

The corrosion progress of steel bridge structures is affected by the environmental parameters. Especially, the amount of chlorides is one of the strongest influence parameters. By monitoring the corrosion of a weathering steel bridge damaged by aerosol chlorides [4], it was observed that the inner surfaces of the bridge cross-section were corroded more severely than the outer surfaces as shown in Fig. 3. The reason was that the

World Academy of Science, Engineering and Technology
International Journal of Structural and Construction Engineering
Vol:11, No:5, 2017

corrosion factors accumulated in the inside of the cross section, i.e. salinities, dusts, moistures, etc., for the duration of the usage. The corrosion thicknesses measured at the surfaces of the monitoring girder in the inside of the bridge cross-section are shown in Fig. 4. In this monitor case, the wind was blowing the aerosol chlorides and the moisture against the bridge from the seaside.
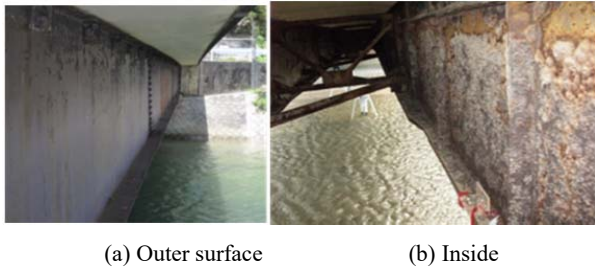

(a) Outer surface   (b) Inside

Fig. 3 Corrosion condition of bridge girders

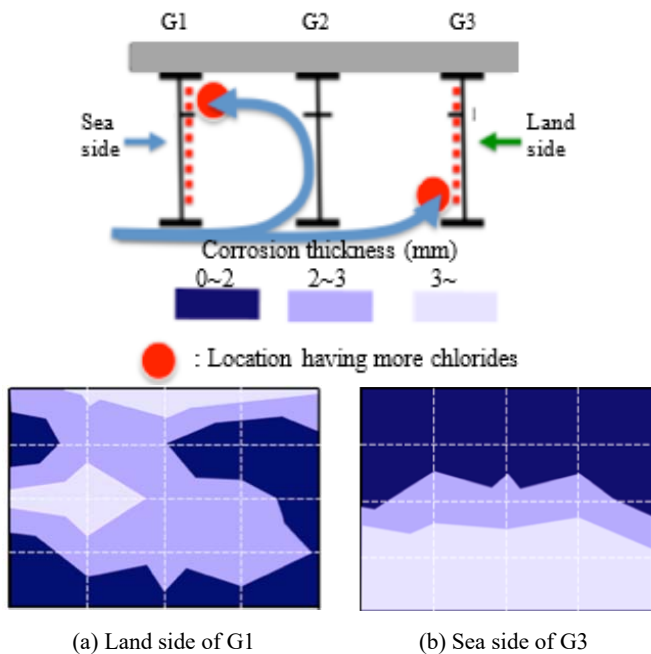
(a) Land side of G1   (b) Sea side of G3

Fig. 4 Corrosion thicknesses of girders monitored

The corrosion thicknesses measured at the surfaces of the monitoring girder in the inside of the bridge cross-section are shown in Fig. 4. In this monitor case, the wind was blowing the aerosol chlorides and the moisture against the bridge from the seaside. The result measured shows that the upper part at the inside of the seaside girder, i.e. at the land side surface of G1 girder and the under the part at the seaside surface of G3 girder were rusty more than the other parts of the measured girders. This corrosion behaviour shows that the part of the wind flow around the girders might blow into the inside of the bridge cross-section as shown in the inset of Fig. 3. Then the aerosol chloride particles transported by the wind accumulate to the inside surfaces of the bridge cross-section and accelerate the corrosion reaction.

B. Confirmation of Wind Flow around Girders

In order to confirm the aerodynamic flow of wind around bridge girders, wind tunnel tests were performed [4]. In the tests, oil mists function as the aerosol chloride particles. The wind tunnel used is an open circuit, blowing down *3.5m* long, and a test section of *1.0 m* wide and *1.0 m* high. Considering the wind tunnel size, the geometric scale of *1:15* model of the monitor bridge structure is selected. The model is made of acrylic resin plates. The model has three girders with *100 mm* of the girder depth, *133mm* of distance between the adjacent girders, and *500 mm* of the girder length. The wind speed of the wind tunnel ranges between *5* and *15 m/sec* that corresponds to *0.3* and *5 m/sec* of the real wind speeds, normally. Reference [4] shows the detail of the test procedures.

Fig. 5 shows typical test result took by a high-speed camera (*2000 flames/sec*). The wind vortexes generate first at the bottom of the windward girder that receives directly the wind attack and, then, engulf the oil mists upward in the inside of the cell composed of girders and deck. The test result shows that the aerosol chlorides are transported in the inside of the cross section of the bridge superstructure by the vertical eddy diffusivity of the wind flow. It can be seen from the result that the test result has confirmed the aerodynamic flow of the wind in the inside of the girder bridge estimated by the corrosion thicknesses measured.
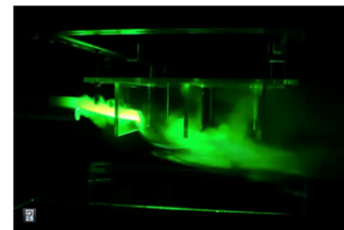
(a) Wind flow aspect around girders
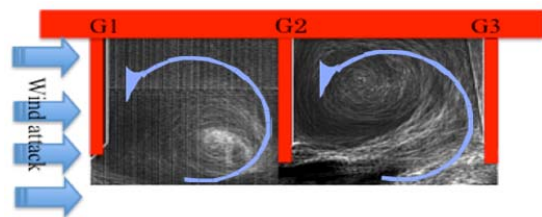
(b) Wind flow aspect in the inside of girders

Fig. 5 Typical result of wind tunnel test

C. Measure for Corrosion Proofing

From the result monitored, the corrosion environment in the inside of the bridge cross-section is dramatically improved by preventing the inflow of the wind vortexes into the bridge cross-section. Considering this essential demand, as a rational measure for the corrosion proofing, a box-shaped girder is proposed, the outer membranes of which are fabricated by stainless steel and the inner members by structural mild steel respectively as shown in Fig. 2.

World Academy of Science, Engineering and Technology
International Journal of Structural and Construction Engineering
Vol:11, No:5, 2017

III. Behaviour of Strength

The buckling strength of formed stainless steel members has been studied regularly and their design specifications are available [5], [6]. Steel bridge superstructures, on the other hand, are fabricated using welded, thin-walled steel plates. However, the welded thin-walled stainless steel members have not been studied sufficiently. The hybrid stainless steel member has been even less. Herein, the ultimate strengths of welded thin-walled austenitic stainless steel members (normal strength material, *SUS304N2A*) composing the hybrid stainless steel girder for bridge construction are examined on the basis of the results obtained so far.

A. Hybrid Stainless Steel Plate Strength

The ultimate compressive strength of the hybrid stainless steel panel, which consists of the stainless steel plates and mild carbon steel stiffener ribs, is evaluated by comparing with the results on the ultimate strengths of generally stiffened stainless steel panel and carbon steel one obtained so far [8], [9].

TABLE I
MATERIAL PROPERTIES

Material	Thickness, t (mm)	Yield strain, %	Yield stress (Mpa)	Tensile strength (Mpa)	Yield ratio	Young's modulus (Mpa)
SUS304-N2A	6	0.313	389	778	0.50	183000
	9	0.318	399	771	0.52	183000
SM490Y	9	0.178	378	531	0.71	212000
SS400	6	0.151	316	456	0.69	209000
	9	0.146	303	448	0.68	207000

Yield stress and strain are evaluated at 0.1% offset strain.

TABLE II
DIMENSIONAL PROPERTIES AND ULTIMATE STRENGTH

Specimen	Plate panel		Rib			Ultimate load	
	T, mm	R	h_r, mm	t_r, mm	γ/γ_{req}	Exp. P_t/P_Y	Ana. P_t/P_Y
HYSS-6.1	6.2	0.68		8.7	1.5	1.03	
-6.2	6.1	0.70		8.6	1.6	1.01	0.94 (t=6mm)
-6.3	6.1	0.70		8.6	1.6	1.02	
SSS-6.1	6.0	0.71	60	9.1	1.7	1.03	-
-6.2	6.0	0.71		9.1	1.7	1.04	-
CSS-6.1	5.8	0.63		8.9	1.8	0.96	-
-6.2	5.8	0.63		8.9	1.8	0.94	-
-6.3	5.8	0.63		8.9	1.8	0.97	-
HYSS-9.1	9.2	0.47		8.6	1.1	1.08	
-9.2	9.3	0.46		8.8	1.1	1.07	1.02 (t=9mm)
-9.3	9.3	0.46	70	8.6	1.1	1.05	
SSS-9.1	9.2	0.47		9.2	1.1	1.14	-
-9.2	9.2	0.46		9.0	1.1	-	-

t=thickness of the stiffened plate, h$_r$ and t$_r$=width and thickness of the rib, Exp.= ultimate load evaluated by experiment, Ana.= ultimate load evaluated by FEM analysis for the hybrid stiffened panel with nominal plate-thickness.

The ultimate strength was tested using the Amsler loading machine of *±2,000k*N and the test arrangement is shown in Fig. 6. Each test specimen for the hybrid stainless steel panels (HYSS series) was composed of stainless steel plate and one longitudinal stiffener rib of *SM490* as shown in the inset (a) of Fig. 7 and was given the boundary condition of stiffened panel by special test-jig as shown in the inset (b) of Fig. 7. The specimens for the generally stiffened stainless steel panels (*SSS* series) or carbon steel ones (*SCS* series) were made up totally of stainless steel of *SUS304N2A* or carbon steel of *SS400*. The properties of the steel materials (*SUS304N2A, SM490, SS400*) were obtained by the metallic material testing and summarized in Table I. Each specimen had the same length of *l=1000mm* and width of *b=350mm*. The plate and the rib were jointed by fillet *MIG* welding with a leg length *4 mm*. The dimensional properties of the test specimens are indicated in Table II.

(a) Amsler test machine　　　(b) Test setup

Fig. 6 Test arrangement

World Academy of Science, Engineering and Technology
International Journal of Structural and Construction Engineering
Vol:11, No:5, 2017
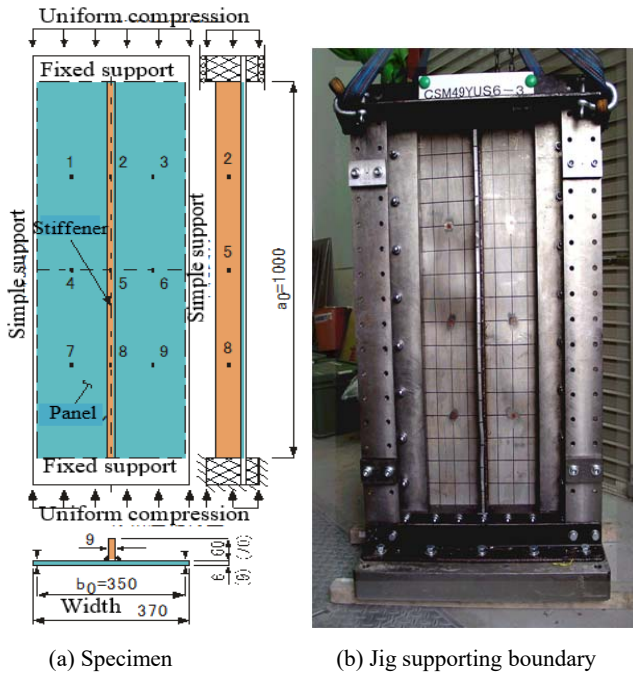
(a) Specimen   (b) Jig supporting boundary

Fig. 7 Test Specimen and its jig

R is the width-thickness parameter and γ is relative stiffness parameter of the longitudinal stiffener, expressed as follows;

$$R = \frac{b}{n \cdot t} \sqrt{\frac{\sigma_y}{E} \cdot \frac{12(1-\nu^2)}{\pi^2 k}} \qquad (1)$$

$$\gamma = \frac{t_r h_r^3}{3} \cdot \frac{bt^3}{11} \qquad (2)$$

in which b is the width of specimen, σ_y is the yield stress shown in Table I where the yield stress of *SUS304N2A* is defined at *0.1%* offset strain, ν is the Poisson's ratio $(=0.3)$, k is the buckling coefficient $(=4)$, E is the Young's modulus of *SUS304N2A* shown in Table I, n is the number of panels separated by stiffeners $(=2)$.

Both ends of each specimen were machined parallel to achieve uniform application of load. The γ_{req} gives the rib rigidity required to retain the node of buckling mode of the stiffened plate and is specified by the *JSSHB, Japan Standard Specifications for Highway Bridges* (Japan Road Association, 2002). The residual stresses and the initial geometric imperfections were measured by releasing the stresses and by sliding the displacement transducers. Reference [8] shows the detail experimental procedures. It was confirmed that the amounts of the residual stress and the geometric imperfection were respectively within the range specified for ordinary steel highway bridge girders by the *JSSHB*.

The ultimate load P_u of each specimen tested is also shown in Table I, P_y of which is the equivalent yield load and expressed as;

$$P_y = b \cdot t \cdot \sigma_y + h_r \cdot t_r \cdot \sigma_{ry} \qquad (3)$$

where σ_{ry} is the yield stresses of stiffener rib, *SM490Y* as shown

in Table I. In this paper, the finite element analysis (FEA) program *MSC. Mark Nastran* [7] was used to confirm the test performance. The real stress-strain property obtained by the coupon test was used in the finite element analysis. The ultimate behaviour of the hybrid stainless steel panels with the nominal plate thicknesses of *t=6mm* and *9mm* was simulated by the FEA. Fig. 8 shows the failure modes obtained by the test and FEA. It is shown that both failure modes appear closed agreement. The ultimate strengths of the hybrid stainless steel panes were compared with those of the generally stiffened steel panels. The tested and analyzed comparisons are shown in Table II in the form of the ultimate strength ratio P_u/P_y. Herein, for practical evaluation, the ultimate strength ratios of the specimens are compared with the generally stiffened carbon steel panel strengths tested to specify the JSSHB [9], [10] as shown in Fig. 9. The compared results clearly show that the ultimate strength ratio of the hybrid stainless steel stiffened panel is almost same degree as the generally stiffened carbon steel panel.

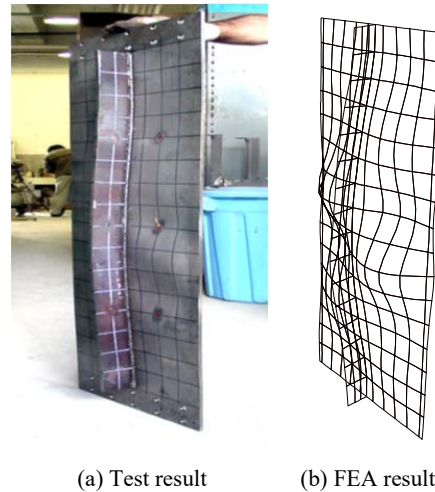(a) Test result   (b) FEA result
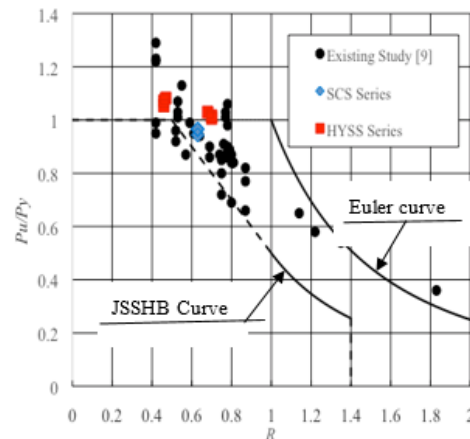
Fig. 8 Failure mode obtained

Fig. 9 Ultimate strength ratio comparisons

B. Flange Plate Strength

The ultimate strength of flange plate of the girder is evaluated by comparing the results on the ultimate strengths of

World Academy of Science, Engineering and Technology
International Journal of Structural and Construction Engineering
Vol:11, No:5, 2017

the welded stainless steel flange plate obtained [11] with the available design specifications [10], [12]. The parametric study on thin-walled, unstiffened stainless steel elements under uniform compression, P_u, that represent flanges of plate girders was examined using the FEA technique to account the geometric and material nonlinearities, the residual stresses, and initial geometric imperfections [11]. The analysis method [7] was validated with experiments on the ultimate strengths of specimens of cruciform shape as shown in Fig. 10 and used to measure the sensitivity of the local geometric imperfection, length-to-width ratio, and slenderness to the compressive capacity of plates, whose boundary conditions simulate the flanges of stainless steel plate girders. The specimen dimensions and the material properties, SUS304N2A, estimated by the coupon tests are presented in Table III. Each specimen had the same length, $a = 800mm$. The λ_f in Table III is the local buckling slenderness parameter for the flange plate defined as;

$$\lambda_f = \frac{b}{t} \sqrt{\frac{12(1-\nu^2)\sigma_y}{E\pi^2 k}} \tag{4}$$

in which vis Poisson's ratio, 0.30 and k is plate buckling coefficient, assumed to be 0.425 for the flange plate. The test arrangement and specimen example tested are shown in Fig. 11. Reference [11] shows the detail of the test procedure.
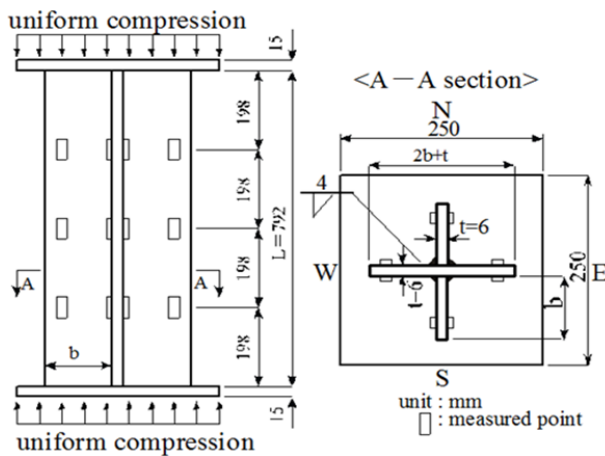

Fig. 10 Details of test specimens

TABLE III
SPECIMEN DIMENSIONS AND MATERIAL PROPERTIES

Specimen No.	t (mm)	b (mm)	λ_f	σ_y Mpa	ε_y %	E_0 Mpa
1	6.21	96.3	1.171	423	0.319	193150
2	6.21	96.3	1.171			
3	6.19	66.5	0.820	436	0.326	192920
4	6.22	66.2	0.813			
5	6.22	47.5	0.587	438	0.327	192951
6	6.21	47.3	0.586			

t=flange thickness, b=flange width, σ_y and ε_y=yield stress and strain evaluated at 0.1% offset strain, E_0=Young's modulus.
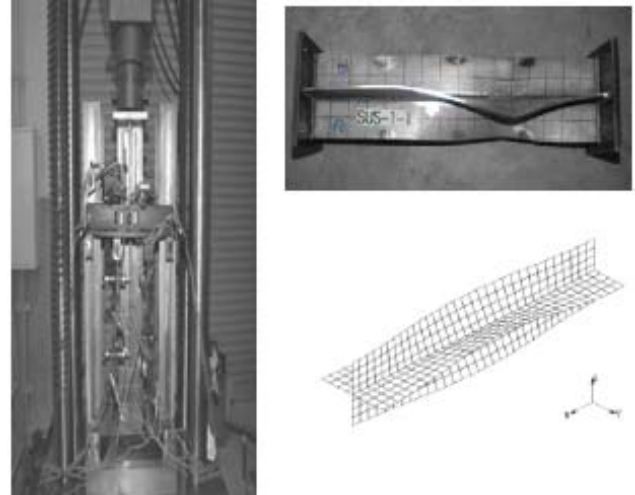

Fig. 11 Test setup and specimen example tested

Table IV compares the yield loads, P_y $(=b \times t \times \sigma_y)$, the ultimate load ratios obtained from the experiment $P_{u, test}$, and from the FEA $P_{u, FEA}$ using the real stress-strain properties determined by the coupon tests. The average discrepancy between the ultimate load capacity results obtained by the analysis and the experimental results is within 3% - reasonably small. The excellent agreement between the measured and computed results indicates that the FEA used is suitable for the buckling analysis of welded stainless steel unstiffened plate elements.

TABLE IV
EXPERIMENTAL AND ANALYTICAL RESULTS

Specimen	P_y kN	$P_{u,FEA}/P_y$ (1)	$P_{u,test}/P_y$ (2)	(1)/(2)
1	1028	0.677	0.679	0.997
2	1028	0.674	0.710	0.949
3	736	1.001	0.988	1.013
4	735	0.948	1.001	0.947
5	535	0.996	1.029	0.968
6	532	1.041	1.052	0.990

The parametric study examined the effect of the combination of the local buckling slenderness parameter defined as (4) and the initial out-of-plane geometric imperfections w_0 on the ultimate strength. The w_0 is assumed to be of sinusoidal shape in the longitudinal direction of x and linear in the width direction of y as follows:

$$w_0 = \overline{w}_0 \left(\frac{y}{b}\right) sin\left(\frac{m\pi x}{a}\right) \tag{5}$$

where $\overline{w}_0$ is a standard value specified in JSSHB, $b/200$ and m is mode value, an integer that varied from 1 to 8 in the parametric study. The material properties used in the parametric study were $E_0 = 1.93 \times 10^5$ Mpa, $\sigma_y = 350Mpa$ and $\varepsilon_y = 0.280\%$, estimated at 0.1% offset strain, which are nominal values by Japan Industrial Standard Specifications. The stress-strain property used was evaluated from the coupon test. The parametric models simulated the compression flange of the plate girder as shown in Fig. 12. The ultimate buckling loads,

World Academy of Science, Engineering and Technology
International Journal of Structural and Construction Engineering
Vol:11, No:5, 2017

P_u, were examined for 140 models. The aspect ratios, a/b, used were 0.5, 1, 2, 4, 6, and 8. Herein, the ultimate load ratios obtained from the specimen tests and FEAs and examined from the parametric studies are compared with the ultimate load ratios of the unstiffened carbon steel elements under uniform compression predicted using the JSSHB [10] and the Eurocode specified by the European Committee for Standardization [12].
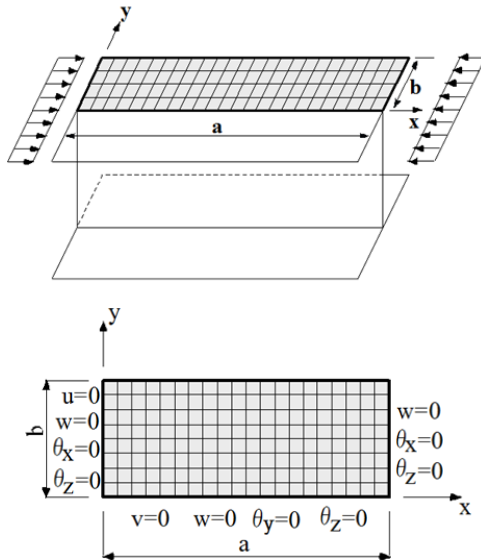

Fig. 12 FEA model of unstiffened flange plate

The comparison is shown in Fig. 13 as the function of the local buckling slenderness parameter for the flange plate. It can be seen from Fig. 13 that the Eurocode design capacity is close to the average of the ultimate loads especially in the range of $\lambda < 1.0$ and JSSHB curve is generally conservative. From the results obtained, it is estimated generally that the ultimate strength ratio of welded, thin-walled, unstiffened stainless steel elements under uniform compression that represent flanges of plate girders is able to be determined by an ordinary design standard for the carbon steel element.
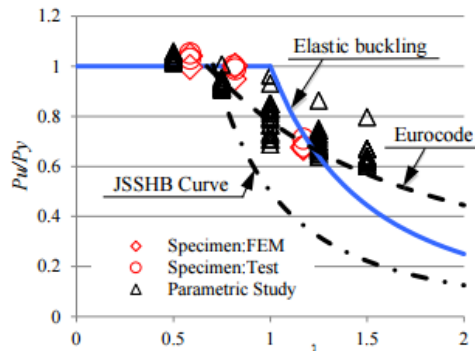

Fig. 13 Ultimate strength comparison of the flange plate

C. Web Plate Strength

The shear strength of the girder is evaluated on the bases of the strength of welded, thin-walled, stainless steel elements that represent webs of plate girders obtained by shear buckling tests

[2]. In the tests, austenitic stainless steel plates, SUS304N2A, *s-series* were used. The ultimate strength results were compared with the buckling test results for the plate girders made of carbon steel SM400, *c-series*. The test results are also compared with the finite element approach FEA solutions [7].

The test girder was composed of three I-girder units – one is a specimen unit and other two are loading units as shown in Figs. 14 and 15. Each girder unit had the same length, *L=1750mm* and web depth, *b=500mm*. The specimen unit configuration provided $\alpha = 1.0$ of the aspect ratio to signify a shear panel length-to-web depth ratio of the test panels. A couple of the shear strength tests were performed for each test series. The detailed dimensions and plate material of the test panels in the specimen units are given in Table V. The web slenderness, λ_w, in the Table V is given as follows:

$$\lambda_w = \frac{b}{t_w}\sqrt{\frac{12(1-v^2)\tau_y}{E\pi^2 k}} \qquad (6)$$

where t_w=web thickness; τ_y=shear yield stress of the web material $(= \sigma_y/\sqrt{3})$; and k=local shear buckling coefficient depending upon the boundary condition (=9.34 for $\alpha = 1.0$)
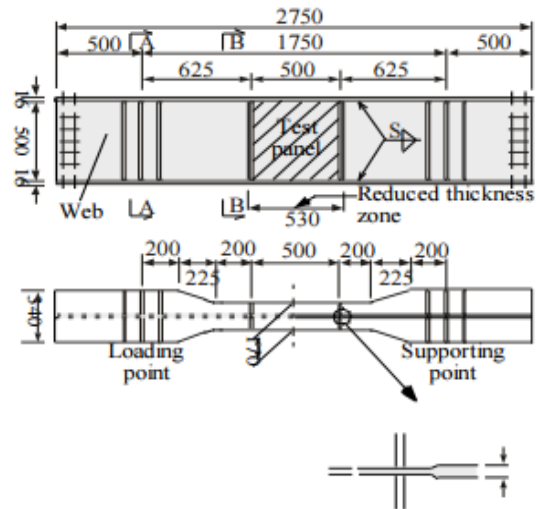

Fig. 14 Specimen unit profile detail

The specimens were tested under two concentrated loads using 1000kN servo-controlled hydraulic jacks as shown in Fig. 16. Each concentrated load was applied through a load cell. Reference [2] shows the detail of the experimental procedures. The ultimate shear strength ratios V_u/V_y obtained from the experiment and the FEA using the real stress-strain properties determined by the coupon tests are compared in Table V, in which $V_y = b \times t_w \times \tau_y$. Typically buckled shapes obtained by the experiment and FEA are shown in Fig. 17. The main object of the comparisons is to check mutually the accuracy of the ultimate strengths obtained. It can be seen that good agreement has been achieved between the experimental and analytical results in all specimens.
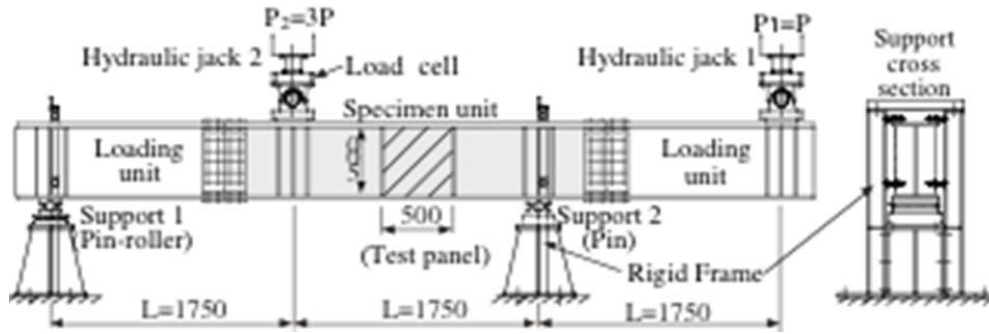
World Academy of Science, Engineering and Technology
International Journal of Structural and Construction Engineering
Vol:11, No:5, 2017

Fig. 15 Test set

TABLE V
SPECIMEN DIMENSIONS, MATERIAL PROPERTIES AND STRENGTHS

Series No.	Steel grade	t_w, mm	Mpa, σ_y	E, Mpa	λ_w	V_u/V_y Test	V_u/V_y FEA
S-32.1	SUS 304N 2A	3.2	399	193000	1.857	0.78	0.78
S-32.2			405	194000		0.70	0.78
S-45.1		4.5	293	213000	1.327	0.85	0.88
S-45.2			309	210000		0.81	0.82
C-45.1	SM 400	4.5	389	212000	1.075	0.85	0.86
C-45.2						0.78	0.81

σ_y for the stainless steel is evaluated at the 0.1% offset strain.
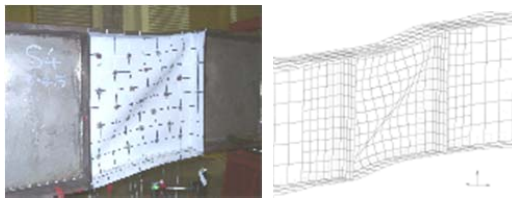

Fig. 16 Loading system

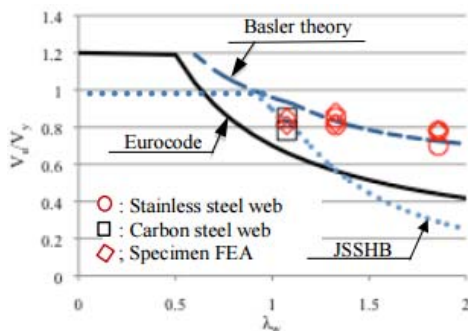Fig. 17 Buckled shapes of stainless steel web plate

Fig. 18 Comparison on ultimate shear strength of stainless steel web plat

The relationship of the ultimate strength ratio V_u/V_y to the buckling parameter λ_w for the all cases examined is shown in Fig. 18. The ultimate load ratio curves by the JSSHB [10], the European Committee for Standardization [13], and the Basler's tension field theory [14] are also shown in Fig. 18 for comparison. The Basler curve is close to the ultimate load ratios obtained in the range of $\lambda_w > 1.3$. The JSSHB curve is close to the ultimate load ratio obtained for $\lambda_w = 1.075$. The Eurocode and JSSHB curves are conservative generally.

IV. COMPARISON OF LIFE-CYCLE COSTS

The life-cycle cost of a bridge structure depends strongly on its maintenance costs. In order to examine the life-cycle cost, the trial calculation of the gross cost, which is the sum of the initial cost and the total amount of the maintenance cost during the usage years, was performed for a model bridge superstructure example shown in the following. The model example is a composite box girder with simple spanning, whose span length is *50m* and bridge width is *10.5m*. The schematics of the cross sections are shown in Fig. 19. A standard carbon steel bridge superstructure composed of two main thin-walled plate girders with the same span length and bridge width as the model example is also examined for comparison. The structural dimensions of the hybrid stainless steel girder were determined by applying the yield stress of the stainless steel estimated at the *0.1%* offset strain to the JSSHB [10]. The weight ratio of stainless steel to carbon steel in the hybrid stainless steel girder was *3* to *2*. The maintenance costs of the carbon steel girders were estimated as repainting every 10 years. The initial and maintenance costs of the girders were calculated, based on the *Quantity Survey Data* provided by the Japan Economic Research Association [15].

World Academy of Science, Engineering and Technology
International Journal of Structural and Construction Engineering
Vol:11, No:5, 2017

(a) Hybrid Stainless Steel bridge
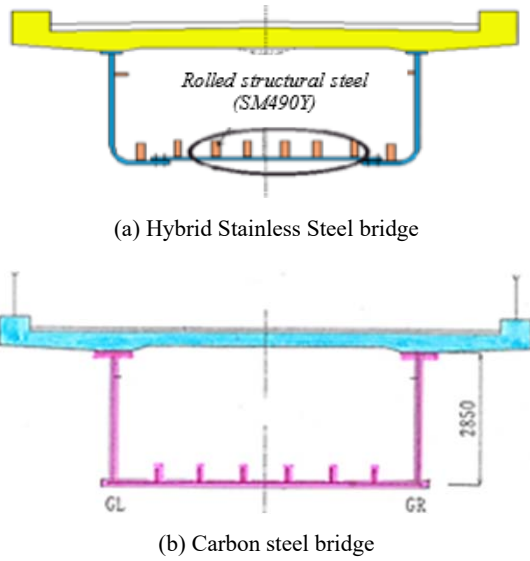

(b) Carbon steel bridge

Fig. 19 Cross section of model bridge girder example

The ratio of the gross cost of each bridge to the initial cost of the standard carbon steel bridge-girder, i.e. cost ratio, is shown in Fig. 20 as a function of the usage year. The initial cost of the hybrid stainless steel girder is 1.4 times as much as that of the standard carbon steel girder. However, carbon steel girders need to repaint periodically so that those gross costs increase with increasing the period of usage. Eventually, in this case, the gross cost of the hybrid stainless steel girder becomes approximately equal to that of the standard carbon steel girder in 35 years.
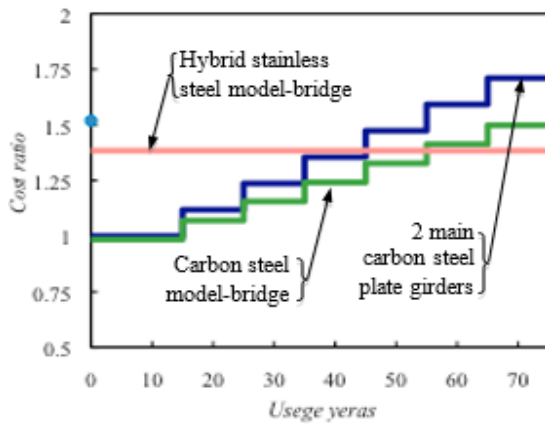

Fig. 20 Comparison of the life cycle cost

V. CONCLUSION

It is found from the results examined that the ultimate strengths of stainless steel members composing the hybrid stainless steel girder for bridge construction can be estimated conservatively by applying the yield stress of the stainless steel at the *0.1%* offset strain to the present specifications. This information promotes the newly convenient design expression to achieve a more efficient use of the stainless steel material in bridge constructions. Furthermore, the trial calculation results on the gross costs of the life-cycle costs demonstrate that the

hybrid stainless girder proposed herein makes it possible to construct a minimum maintenance bridge especially in local areas.

The high costs and the lack of structural specifications that conveniently predict the actual strength of stainless steel as structural materials have led a limited use of stainless steel in bridges despite exhibiting excellent material properties and aesthetics. The results examined on the hybrid stainless steel girder in this paper have been shown to be an efficient solution to the above issue.

REFERENCES

[1] H. Kuwamura, A. Isozaki, "Local buckling and effective width of thin-walled stainless steel members," in *Proc. 3rd Int. Conf. Thin-Walled Structures*, Cracow, Poland, 2001, pp. 209–216.
[2] T. Yabuki, Y. Arizumi, H. Matsusita, S. Guezoeli, "Buckling Strength of Welded Stainless Steel Girder Webs in Shear," in *Proc. Int. Coll. Stability and Ductility of Steel Structures,* Lisbon, Portugal, 2006, pp. 811–818.
[3] I. Estrada, E. Real. E. Mirambell, "Shear resistance in stainless steel plate girders with transverse and longitudinal stiffening,*" J. Constructional Steel Research,* vol. 64, Issue 11, pp. 1239–1254, Nov. 2008.
[4] T. Yabuki, Y. Arizumi, T. Shimozato, S. Yamashita, "Smart FRP usage for prevension in steel girder bridge against chloride attack," in *Proc. 6th Int. Conf. FRP Composites in Civil Engineering*, Roma Italy, 2012, No. 13–166.
[5] American Society of Civil Engineers, "Specification for the Design of Cold-Formed Stainless Steel Structural Members", *SEI/ASCE-8-02*, Virginia, USA, 2002.
[6] Australia/New Zealand, "Cold-Formed Stainless Steel Structures" *AS/NZS 4673, Standards Australia*, Sydney, Australia, 2001.
[7] Mark/Standard User's Manual 2001, MSC Software, Inc.
[8] H. Matsusita, T. Yabuki, Y. Arizumi, S. Iwata, "An experimental study on ultimate compressive strength of stainless steel plates stiffened with mild carbon steel ribs," in *Proc. Int. Conf. Advances of Experimental Structural Engineering,* Nagoya, Japan, 2005, pp. 99–106.
[9] M. Kanai, A. H-S. Ang "A Study of Safety of Box Girder Bridges in Japan*" Structural Research Series No.475* 、 Civil Engineering Department, University of Illinois, 1979.
[10] Japan Road Association, "*Japan Standard Specifications for Highway Bridges*", 2002.
[11] T. Yabuki, Y. Arizumi, T. Shimozato, S. Guezoeli, "Ultimate Compression Load of Stainless Steel Flange Plates," in *Proc. 5th Int. Conf. Thin-Walled Structures*, Brisbane, Australia, 2008, pp. 891–898.
[12] European Committee for Standardization, 2004.
[13] European Committee for Standardization ENV, 1993.
[14] T. V. Galambos (ed.), "Guide to Stability Design Criteria for Metal", *SSRC, John Wiley & Sons,* New York, 1998. 1993.
[15] Japan Economic Research Association, "*Quantity Survey Data, 2015*".